Locating scatterers ahead of a tunnel boring machine using noise correlation

U. Harmankaya, A. Kaslilar, K. Wapenaar, and D. Draganov

Summary
The investigation and detection of faults, fractures, karst zones, cavities, etc., is important to reduce hazardous risks, in particular during excavation with tunnel boring machines. To locate such scatterers, we propose a method based on seismic interferometry that uses the noise signals generated by a TBM. Using finite-difference modelling of TBM noise in a homogeneous half-space, we model noise recordings. We then correlate the noise to obtain non-physical scattered arrivals for various scatterer locations. We use both non-physical scattered P- and S-wave arrival times to successfully estimate the location of scatterers.

Introduction

Optimization of tunnelling projects for technical, environmental, cost- and timesaving aspects generally require detailed knowledge of geological conditions of the area where the tunnelling is planned. Thus, detection of relevant faults, fractures, karst zones, water- or gas-bearing zones, cavities, and different kind of soft ground becomes very important for reducing hazardous risks, in particular during excavation with tunnel boring machines (TBM) (Kaus and Boening, 2008). This created the need for methods that can "look ahead", i.e., detect any abrupt changes within the subsurface ahead of the TBM. Several geophysical methods are used to address this problem. These include geoelectical (Kaus and Boening, 2008, Kopp, 2012), ground penetrating radar (Richter, 2008) and seismic methods (Brückl et al., 2001, Sattel et al., 1992, Swinnen, 2007). While active-source seismic methods are more widely used in seismic exploration, recent years saw a surge in interest for passive-source seismic methods. Hauser (2001) was the first to successfully locate an obstruction ahead of a tunnel route using vibrations of a TBM. In that study, correlated noise recordings indicated the presence of a scatterer, which was also confirmed with ray-tracing modelling.

In this study, we consider the method described in Harmankaya et al. (2013) that uses non-physical arrivals to determine the location of a scatterer. While the method was originally developed for active-source seismic records, it is shown here that it can also be applied with a few modifications to passive seismic records. Here, the method is tested on three different scatterer locations using scattered P- and S-wave arrivals separately. It is observed that in all cases reliable estimations for scatterer locations are obtained.

Estimation of the Location of the Objects by Non-physical Scattered Waves

We aim to estimate the location of scatterers present along the path of a TBM by using the method described by Harmankaya et al. (2013). This method uses cross-correlation and inversion to estimate the location of a diffractor or scatterer. This method was previously applied to active-source seismic data (Kaslilar et al, 2013), but here we use noise as a source. Passive seismic modelling was conducted using 2D finite-difference modelling program (Thorbecke and Draganov, 2011), which is capable of simulating active or passive sources. Figure 1 shows the model geometry where the TBM is indicated by a tan rectangular area at a depth of 18 meters, having 1 m width and 6 m height. We consider three scatterer locations (*sc1*, *sc2,* and *sc3*), which are ahead of the TBM at depths of 25 m, 19 m and 13 m, respectively. Two of the scatterers are located below and above the TBM, to represent various locations for a cavity or any other object that could threaten the tunnelling operations.

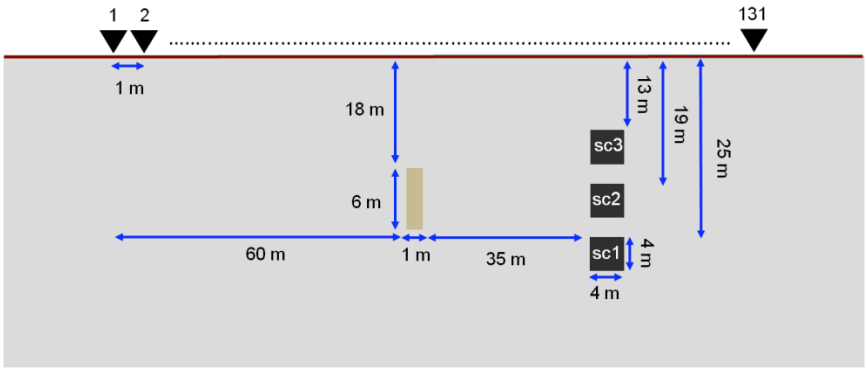

Figure 1 *Schematic view of the model: noise source area representing a TBM (tan rectangle), receivers (triangles) and scatterers (black squares). Background P-wave velocity (V_P) is 600 m/s, while S-wave velocity (V_S) is 350 m/s.*

The three scatterers are modelled independently. Wavefields are recorded by 131 receivers located at the surface and spaced at 1 m. For the passive modelling, the TBM noise is represented by 20 random noise sources located randomly inside the rectangular tan area. The noise's maximum frequency is

150 Hz, average duration of each source signal is 50 s, while the total duration of the modelling is 180 s. Figure 2a shows the recorded wavefield for the modelling for scatterer *sc2* (due to limited space, images from other cases are not shown). We select a virtual-source (VS) location at receiver 20 (19 m) and cross-correlate all the traces from Figure 2a with the trace at the VS location to obtain Figure 2b. Here, both physical and non-physical arrivals may be present. In Figure 2b, we focus on the scattered P- and scattered S-waves and isolate them for further processing (Figure 2c and 2d). Because the VS is to the left of the TBM and the scatterer, these scattered arrivals are non-physical.

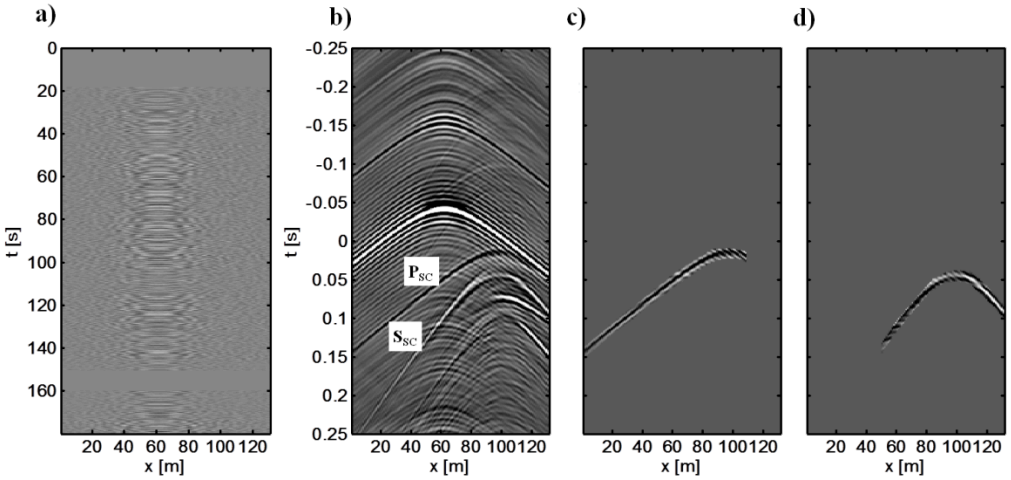

Figure 2 *(a) Recorded wavefield from noise sources for scatterer sc2. (b) Correlated wavefield for virtual source 20 (VS20). (c) and (d) Isolated P-wave and S-wave scattered arrivals from correlated wavefield (b).*

To apply the method given in Harmankaya et al. (2013), we need the travel paths between the scatterer and the receivers. To provide this, we choose VS locations and apply a second cross-correlation to all the traces with the trace at the VS location but now using only the wavefields in Figure 2c and 2d. In this way, the dependence of the travel-time differences obtained from the first correlation on the TBM location is eliminated, and non-physical scattered arrivals are obtained, which depend only on the scatterer location. As the location of the scatterer does not change, the arrival times from the scatterer to the receivers are always constant (stationary), irrespective of the path to the scatterer. The isolated and cross-correlated scattered P-waves for virtual-source location VS30 (29 m) are shown in Figure 3a and b, while the S-wave results for VS79 - in Figure 3c and 3d. For the subsequent inversion, only the travel times from Figure 3b and 3d to obtain the location of scatterers.

To estimate the location of a scatterer, the following non-physical travel-time relation is used (Harmankaya et al, 2013):

$$t = \frac{1}{V}\left\{\left[\left(x_i^r - x\right)^2 + \left(z_i^r - z\right)^2\right]^{1/2} - \left[\left(x_{vs} - x\right)^2 + \left(z_{vs} - z\right)^2\right]^{1/2}\right\}. \quad (1)$$

The relation calculates non-physical (ghost) traveltimes between the VS, the scatterer, and the receivers. In Eq. (1), V is the wave velocity, i is the index for the receiver numbers, r and vs denote the receiver and virtual source, and x and z are the horizontal and vertical coordinates of a scatterer. The traveltime relation Eq. 1 is used in an inversion to estimate the unknown model parameters (the x and z location of the object) from the observed traveltimes obtained for each VS location. The weakly nonlinear problem is solved iteratively by using damped singular value decomposition (Harmankaya et al, 2013). The uncertainties of the estimations are obtained by the model covariance matrix using a coverage factor 2, which provides a confidence level of 95 %.
As can be seen from Figure 2, the cross-correlation of the noise signal yielded scattered arrivals that are relatively easy to select from the rest of the recorded wavefields, as there is only one scatterer in

each modeling case. Multiple scatterers, especially located close to each other, could make selecting the correct traveltimes more difficult. Here, the traveltimes are easily obtained from the non-physical arrivals shown in Figure 3b and 3d. For each scatterer location, only one set of virtual sources are used, which are VS30 and VS79 for P and S wave arrivals, respectively.

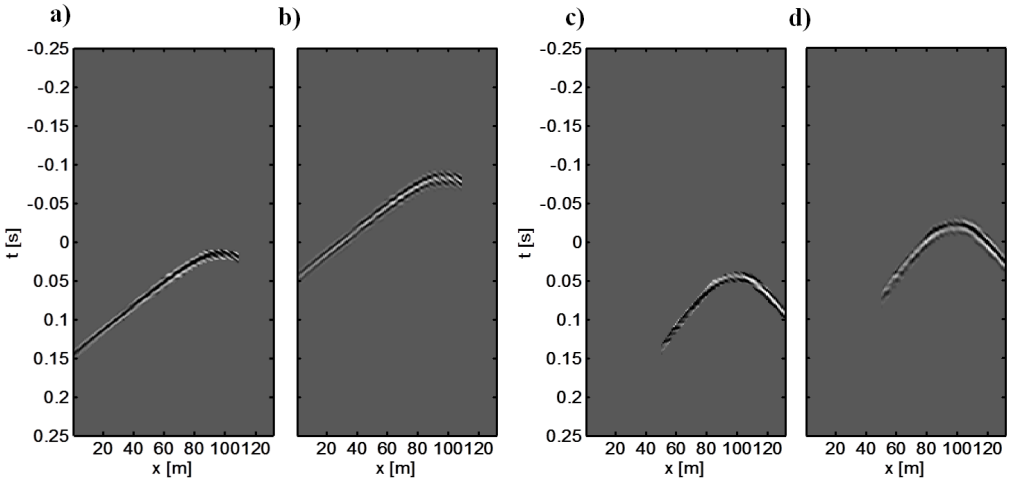

Figure 3 *(a) and (c) Repeated from Figure 2c and 2d, respectively. (b) and (d) Cross-correlation of the P- and S- wave arrivals given in (a) and (c), respectively, with the trace at VS30 (29 m).*

Results of the inversion for P wave arrivals are given in Figure 4. In Figure 4a, the fit between observed (dots) and calculated (lines) traveltimes for each scatterer location (1, 2 and 3 for *sc1*, *sc2* and *sc3*, respectively) are shown. The initial and the updated model parameters, *x* and *z* locations of a scatterer, are given for each iteration in Figure 4b. After five iterations, the locations of the scatterers are estimated accurately. The results are also listed in Table 1. The errors in traveltimes (E_t) are calculated as $E_t = \left[\sum (t_o - t_c)^2 / \sum (t_c)^2\right] \times 100$, where t_o and t_c represents observed and calculated traveltimes, respectively, and N – number of observations. The errors in the model parameters are calculated by $E_m = \left|(m_a - m_e)/m_a\right| \times 100$, where m_a and m_e are the actual and estimated model parameters *x* and *z*. It should be noted that the error calculations of the model parameters are made relative to the center point of the scatterers. From the results in Table 1, we can conclude that the locations of the scatterers are estimated with less than 7% error.

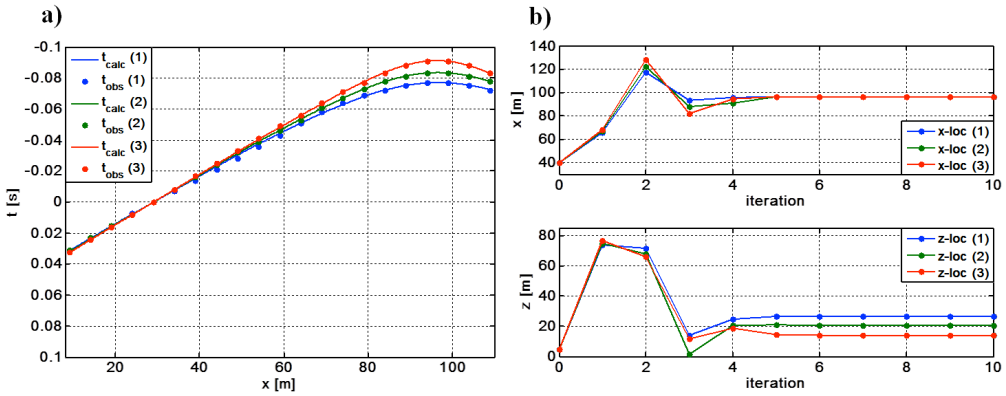

Figure 4 *Inversion result for scatterer sc1 (blue), sc2 (green), and sc3 (red). (a) Observed (dots) and calculated (solid line) traveltimes; (b) Estimated horizontal and vertical locations (x and z) of the scatterers in each iteration. The values at the zeroth iteration correspond to the initial parameters for the inversion.*

Table 1 *Estimated model parameters for different scatterer locations (sc1, sc2 and sc3) for the configuration given in Figure 1. The actual location of the scatterer (AL), the estimated model parameters (x and z) with their 95% confidence levels (1.96 σ), percentage errors on the travel times (E_t) and model parameters (E_m) are also given.*

		AL (m) x/z	x±σx	z±σz	E_m (%) x/z	E_t (%)
P - wave	sc1	98.00/27.00	96.71±1.20	26.63±1.77	1.31/1.37	0.034
	sc2	98.00/21.00	96.53±0.57	20.50±0.82	1.50/2.38	0.009
	sc3	98.00/15.00	96.28±0.42	13.96±0.63	1.71/6.93	0.007
S - wave	sc1	98.00/27.00	96.44±0.42	28.65±1.09	1.59/6.11	0.056
	sc2	98.00/21.00	96.32±0.30	22.01±0.76	1.71/4.81	0.032
	sc3	98.00/15.00	96.36±0.21	14.82±0.53	1.67/5.00	0.017

Conclusions

Using a method inspired by seismic interferometry, we showed that from the correlation of noise records from a tunnel boring machine, we can estimate the location of the scatterers ahead of the machine. For this, we use scattered body-wave noise and two correlations. With clearly observable scattered arrivals, we obtain very good estimations of scatterers at varying depths. We foresee that this method, after further tests and possible improvements, can be a useful tool for tunnelling projects.

References

Brückl, E., Chwatal, W., Dölzlmüller, J., Obstl, W. J. [2001] A study of the application of VSP to exploration ahead of a tunnel. *International Journal of Rock Mechanics & Mining Sciences*, **38**, 833-841.

Harmankaya, U., Kaslilar, A., Thorbecke, J., Wapenaar K. and Draganov, D. [2013] Locating near-surface scatterers using non-physical scattered waves resulting from seismic interferometry. *Journal of Applied Geophysics*, **91**, 66-81.

Hauser, E.C. [2001] Detection and Location of Obstructions Ahead of a Tunnel Boring machine using the Tunneling Vibrations as a Seismic Source -- The First Successful Example. *2001 Symposium on Application of Geophysics to Environmental and Engineering Problems (SAGEEP)*, 2001 CD Publication SSI-7, 6p.

Kaslilar, A., Harmankaya, U., Wapenaar, K. and Draganov, D. [2013] Estimating the location of a tunnel using correlation and inversion of Rayleigh wave scattering. *Geophysical Research Letters*, **40**(23), 6084-6088.

Kaus, A., Boening, W. [2008]. BEAM - Geoelectrical Ahead Monitoring for TBM-Drives. *Geomechanics and Tunneling*, **1**(5), 442-450.

Kopp, T. [2012] Real-Time Monitoring of Geological Conditions During Mechanized Tunneling by Means of Beam4 Method. *Proc. 1st Eastern European Tunneling Conference*, Budapest, Hungary, Aug. 18-21.

Richter, T., Kirschke, D., Jäkel, M. [2008] Geophysical Investigations in Advance and of the Surrounding Karstified Rock During the Construction of the "Katzenberg Tunnel" in Germany. *Geomechanics and Tunnelling*, **1**(5), 450–459.

Sattel, G., Frey, P., and Amberg, R. [1992] Prediction ahead of the tunnel face by seismic methods, pilot project in Centovalli Tunnel, Locarno, Switzerland. *First Break*, **10**, 19–25.

Swinnen G., Thorbecke, J.W., Drijkoningen, G.G. [2007] Seismic imaging from the TBM. *Rock Mechanics and Rock Engineering*, **40**, 577-590.

Thorbecke, J., Draganov, D. [2011] Finite-difference modeling experiments for seismic interferometry. *Geophysics*, **75**, H1-H18.